FERMION PAIR PRODUCTION AT LEP2

STEPHAN WYNHOFF

III. Phys. Institut, RWTH-Aachen, 52056 Aachen, Germany
E-mail: Stephan.Wynhoff@cern.ch

In this article results from LEP at centre-of-mass energies from 130 GeV to 189 GeV given by the experiments ALEPH, DELPHI, L3 and OPAL are summarised. The measured cross sections and forward-backward asymmetries for lepton pair production and pair production of b and c quarks as well as the inclusive hadronic cross section are presented. These data are used to constrain the interference between photon and Z exchange in the S-Matrix framework and to investigate the running of the electromagnetic coupling constant α. Furthermore limits on a hypothetical additional vector boson Z′ and lower limits on deviations from the standard model in the framework of contact interactions are given.

1 Measurement of cross sections and forward-backward asymmetries

1.1 Introduction

Since 1995 LEP has been operated at centre-of-mass energies, $\sqrt{s}$, well above the Z-resonance. This allows to study fermion pair production in e^+e^- collisions up to $\sqrt{s}$ ≈189 GeV. The bulk of the data available has been taken at $\sqrt{s}$ ≈183 GeV. In Table 1 the integrated luminosities per experiment at the different centre-of-mass energies are summarised. While the results from older data are partially published, the analyses of the 189 GeV data are preliminary [1,2,3,4].

Year	$\sqrt{s}$ [GeV]	$\mathcal{L}$/Exp. [pb^{-1}]	qq stat.err. [%]
1995 & 1997	130	~ 6	2.2/4.7
1995 & 1997	136	~ 6	2.5/5.3
1996	161	~ 10	2.6/5.8
1996	172	~ 10	2.8/5.8
1997	183	~ 55	1.3/2.9
1998	189	30-40 (150)	(0.8/1.7)

Table 1: Integrated luminosity per experiment and centre-of-mass energy. For 1998 the expected total numbers are given in brackets.

1.2 Fermion pair production at high energies

A striking feature of fermion pair production at centre-of-mass energies above the Z-Resonance is the presence of hard initial state Bremsstrahlung (ISR). In a large fraction of the events one or several photons are radiated from the incoming electron or positron with a total energy, E_γ, and momentum vector, $\mathbf{P}_\gamma$, such that the annihilation process takes place at a reduced centre-of-mass energy $\sqrt{s'}$. The $\sqrt{s'}$ value is given by:

$$s' = s - 2E_\gamma\sqrt{s} + E_\gamma^2 - \mathbf{P}_\gamma^2\,. \tag{1}$$

Since Bremsstrahlung photons are predominantly produced collinear to the emitting particle, most of them escape undetected along the beam pipe and their momentum has to be infered exploiting kinematic constraints. There exist basically two different methods: Firstly, a kinematic fit assuming one ore more photons ($\Delta\sqrt{s'}/\sqrt{s'} \approx 10\%$) and secondly, the reconstruction from the jet or particle angles assuming one photon exactly along the beam axis ($\Delta\sqrt{s'}/\sqrt{s'} \approx 15\%$). When the photon is detected in the electromagnetic calorimeter and for the e^+e^- final state L3 can measure $\sqrt{s'}$ with a resolution $\Delta\sqrt{s'}/\sqrt{s'} \approx 4\%$. Figure 1 shows the distribution of $\sqrt{s'}$ at $\sqrt{s} = 189$ GeV for hadrons as measured by the OPAL collaboration and determined using a kinematic fit procedure. Two well separated peaks are observed: One at $\sqrt{s'} \approx m_Z$ and one at $\sqrt{s'} \approx \sqrt{s}$. The experiments give two sets of cross sections and forward backward asymmetries for each centre-of-mass energy point. One for the inclusive sample, i.e. events with $\sqrt{s'/s} > 0.1$ (DELPHI: $\sqrt{s'} > 75$ GeV) and one for non-radiative events with $\sqrt{s'/s} > 0.85$ (ALEPH: > 0.90). The measurements for non-radiative events are used to search for new

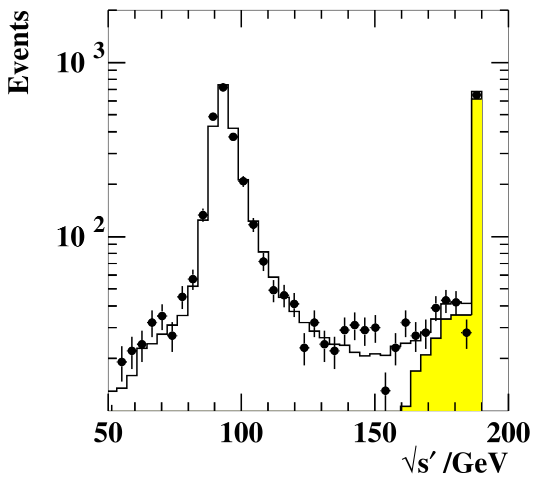

Figure 1: Distribution of the effective centre-of-mass energy for hadrons at $\sqrt{s} = 189$ GeV as measured by OPAL.

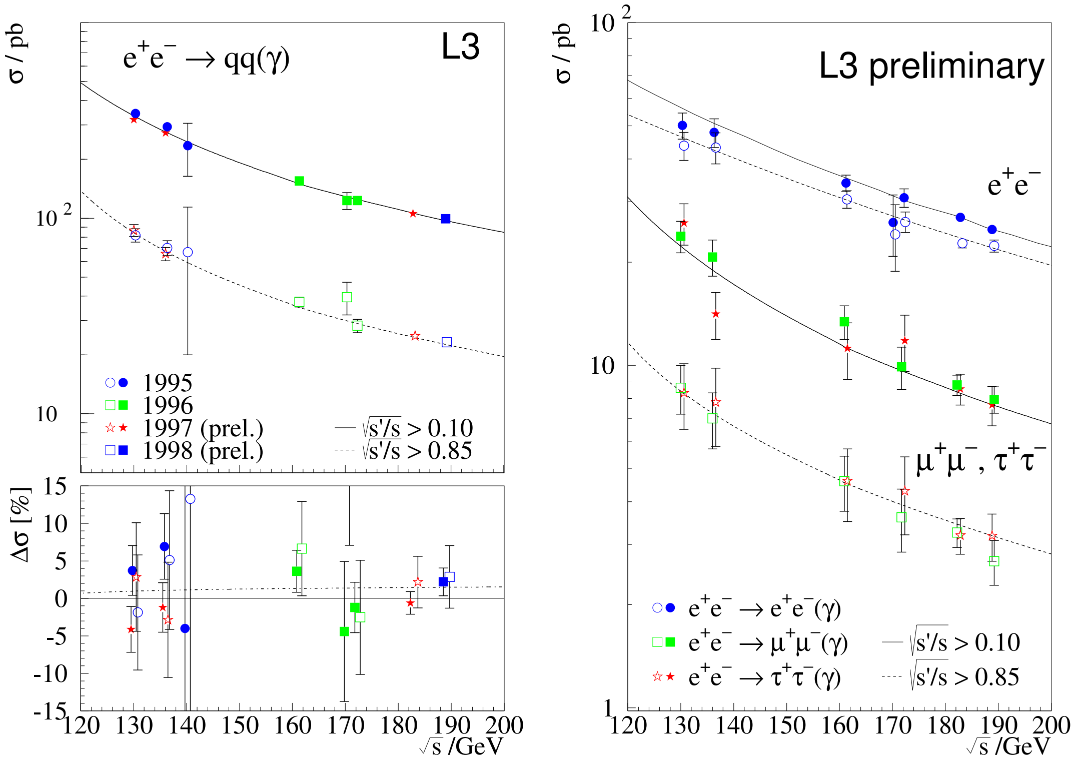

Figure 2: Cross sections for fermion pair production at centre-of-mass energies above the Z resonance measured by L3. The lines represent the Standard Model predictions for the inclusive (solid line) and the non-radiative (dashed line) event sample. The lower plot on the left shows the difference between the measurement and the SM. Here the dashed line shows the difference between the SM prediction with and without interference effects for $\sqrt{s'/s} > 0.85$.

physics phenomena since for these events the annihilation process takes place at the full centre-of-mass energy. The definition of $\sqrt{s'}$ however is meaningless when taking into account the interference between initial and final state radiation. With the increased statistical significance of last years and this years datasets the interference effect gains in importance. Often the experiments use $\sqrt{s'}$ as a symbol when they actually mean the invariant mass of the produced fermion anti-fermion pair, being a experimentally unambiguously defined quantity. The interference effect is only of importance for the non radiative event sample. Its size is about 1% to 2% for $\sqrt{s'/s} > 0.85$ at $\sqrt{s} = 183$ GeV, depending on the final state. The effect increases slightly with energy and is most prominent for large values of $|\cos(\vartheta_f)|$. ALEPH consequently reduces the interference effect (which is larger for their cut of $\sqrt{s'/s} > 0.90$) by restricting the polar angular range of the events to $|\cos(\vartheta_f)| < 0.95$. OPAL is correcting their measurements to 'no-interference' ($\mathcal{O}(\alpha)$) to facilitate the comparison with new physics theories where usually interference effects are neglected.

Another point of interest is the treatment of 4-fermion events. An ISR photon in the event can split into a second fermion anti-fermion pair. Mostly this second pair will have very low invariant mass and not even be resolved in the detector. These events are considered as signal. At centre-of-mass energies greater than about twice m_Z four fermion final states can occur via the production of two real Z bosons. These events however are considered as background.

All four LEP experiments measure the cross section for both event samples in the channels $e^+e^- \to q\overline{q}(\gamma)$, $e^+e^- \to \mu^+\mu^-(\gamma)$, $e^+e^- \to \tau^+\tau^-(\gamma)$ and $e^+e^- \to e^+e^-(\gamma)$ where the (γ) indicates the presence of one or more photons. The results of L3 are shown in Fig. 2. The agreement between the measurement and the Standard Model (SM) prediction, shown as lines, is good both for hadron and for lepton production. Measuring the charge of the leptons the experiments determine forward backward asymmetries. These show also – within their larger statistical errors – similar agreement between data and the SM.

1.3 Measurement of heavy flavour production

ALEPH, DELPHI and OPAL apply also flavour tagging on the hadronic events to determine cross sections or branching ratios ($R_q = \frac{\sigma_q}{\sigma_{\rm had}}$) and quark charge (ALEPH) or forward backward (DELPHI, OPAL) asymmetries for $b\bar{b}$ and $c\bar{c}$ production[1,2,5]. In Table 2 measured values for R_b are shown. The measurements confirm the predicted energy dependence for R_b and R_c. While the value of R_b drops compared to the value on the Z resonance, that for R_c raises slightly.

ALEPH	0.151±0.024
DELPHI	0.142±0.024
OPAL	0.168±0.025
LEP	0.154±0.014

Table 2: Measured values for R_b from 161 GeV and 172 GeV data combined. The errors are statically only, systematic errors are small and not taken into account for the average. The SM prediction is $R_b = 0.165$.

2 Interpretation within the Standard Model

While on the Z resonance the total cross section was strongly dominated by Z exchange, at higher energies the sensitivity for the photon exchange and the γ/Z interference is increased since the fraction of Z mediated events drops rapidly. It is obvious that the non-radiative event sample is the suitable choice to study γ exchange and γ/Z interference and consequently only these are used for the analyses presented in this section.

2.1 Running of α

For muon and tau final states with $\sqrt{s'} \approx \sqrt{s}$ the contribution of γ exchange to the cross section which is proportional $\alpha^2(Q^2)$ is two to four times larger than that of Z exchange. For hadronic final states even at highest energies the Z exchange is still dominating and only a small sensitivity on $\alpha(Q^2)$ remains. OPAL does a χ^2 fit to the non-radiative cross section and forward backward asymmetry measurements within the Standard Model varying $\alpha(Q^2)$ as only free parameter[4] (m_H = 300 GeV). In Fig. 3 the open circles show the result for the different centre-of-mass energies. Combining all data results in the black dot and in a value $1/\alpha(169.34\text{GeV}) = 127.8^{+4.1}_{-3.6}$, which nicely agrees with the predicted energy dependence of the electromagnetic coupling constant. One has however to be aware of the correlation between α and e.g. m_H. For the fit the energy dependence of α is assumed for the luminosity measurement, i.e. up to $Q \approx 3.5$ GeV. An alternative fit using ratios of cross sections and thus avoiding this problem gives a compatible result with a slightly larger error.

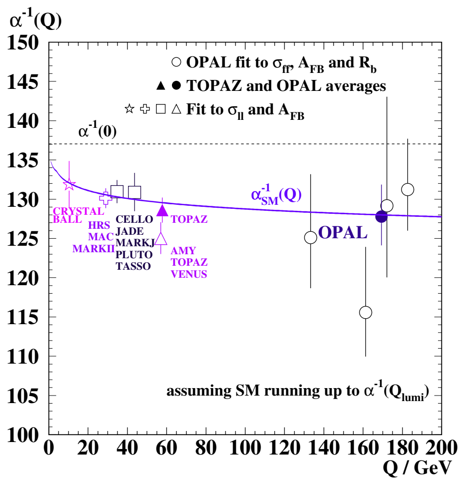

Figure 3: Energy dependence of the electromagnetic coupling constant α as measured by the OPAL experiment. For comparison measurements at lower $\sqrt{s}$ are also shown. The solid line represents the Standard Model expectation, while the dashed line shows the value of $1/\alpha(0)$.

2.2 Determination of the γZ interference

In a similar way the high energy data allow to access the γ/Z interference. An S-matrix ansatz[6], which makes a minimum of theoretical assumptions, is used. In lowest-order the total cross section, σ^0_{tot}, is given by formula (2), where the parameters r_f, j_f and g_f scale the Z exchange, γ/Z interference and γ exchange contributions, respectively.

$$\sigma^0_a(s) = \frac{4}{3}\pi\alpha^2 \left[\frac{g^a_f}{s} + \frac{s r^a_f + (s - \overline{m}^2_{\text{Z}}) j^a_f}{(s - \overline{m}^2_{\text{Z}})^2 + \overline{m}^2_{\text{Z}} \overline{\Gamma}^2_{\text{Z}}} \right] \; ; \quad a = \text{tot}, \text{fb} \tag{2}$$

The S-matrix parameters are determined in a χ^2 fit to the non-radiative data and that collected on the Z-pole by

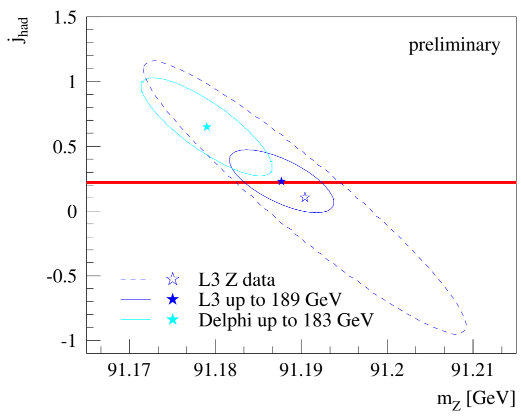

Figure 4: Correlation contour at 68% C.L. between m_Z and j_{had}. The horizontal band corresponds to the SM prediction for j_{had}

DELPHI[2] and L3[3]. The result of the fit (see Table 3) is in good agreement with the SM prediction of $j_{\text{had}} = 0.22$. Compared to the Z-pole data alone, the error is reduced by a factor of 3-4. In Fig. 4 the resulting contour in the $m_Z - j_{\rm had}$ plane is shown. Due to the correlation between $j_{\rm had}$ and m_Z this causes an additional error on the Z mass. This uncertainty is diminished according to the improved knowledge of $j_{\rm had}$.

data used	$j_{\rm had}$	m_Z [MeV]
L3, Z-pole	0.18 ± 0.73	91188 ± 3 ± 13
L3, → 189 GeV	0.23 ± 0.16	91188 ± 3 ± 2.7

Table 3: Result for $j_{\rm had}$ and m_Z from a fit within the S-matrix framework to the data collected on the Z-pole and including the data collected with $\sqrt{s'/s} > 0.85$.

3 Search for new physics phenomena

Although the Standard Model describes the experimental data extremely well, the search for new phenomena based on a more fundamental theory becomes more exciting with increasing centre-of-mass energies. Here two such models will be discussed: The assumption of an additional vector boson Z′ and the more general framework of contact interactions.

3.1 Additional vector boson Z′

An additional vector boson Z′ can be introduced into the SM by modifying its Lagrangian to $\mathcal{L} = eA_\mu J^\mu_\gamma + gZ_\mu J^\mu_Z + g'Z'_\mu J^\mu_{Z'}$. It is characterised by its mass $m_{Z'}$ and a mixing angle $\theta_{\rm M}$ between the Z and the Z′ bosons. Its existence modifies for instance the ρ parameter according to Eq. 3

$$\rho_f \to \rho_f \left(1 + \frac{m^2_{Z'}}{m^2_Z}\sin^2\theta_{\rm M}\right) \tag{3}$$

Precision measurements on the Z pole are sensitive to $\theta_{\rm M}$. Above the Z resonance the contributions due to a Z′ propagator could become important. The most simple model for a Z′ is the Sequential Standard Model (SSM) where the Z′ is postulated to have SM couplings. Besides that models resulting from E_6 GUT (characterised by the parameters χ, ψ or η) or left-right symmetries [7] are studied at LEP by DELPHI [2] and L3 [8]. In Figure 5 the allowed regions for the χ, ψ, η and LR model as determined by L3 including the data at $\sqrt{s} = 189$ GeV are shown. While for $|\theta_{\rm M}| > 0.005$ the existence of a Z′ is ruled out for all masses, for small mixing the lower mass limit depends on the model. A comparison of the DELPHI and L3 results with those of direct measurements at Tevatron [9] is given in Table 4. While for the GUT and LR models CDF obtains more stringent limits due to the higher accessible centre-of-mass energies, the best limit in the SSM is set by L3, excluding masses for the Z′ below 820 GeV.

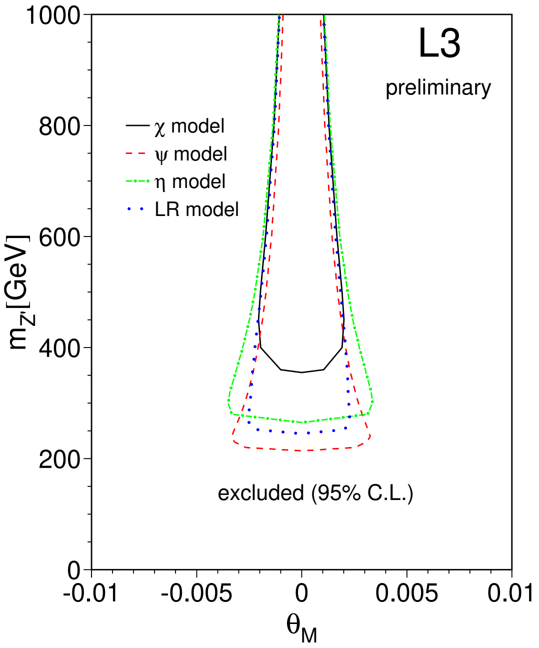

Figure 5: The 95% C.L. allowed regions in the $m_{Z'}$-$\theta_{\rm M}$ plane for the χ, ψ, η and LR model as determined by L3.

3.2 Contact interactions

In the framework of four fermion contact interactions deviations from the SM are characterised by a coupling strength, g, and an energy scale, Λ. At energies much lower than Λ, the exchange of virtual new particles is described by an effective Lagrangian [10]:

$$\mathcal{L} = \frac{1}{1+\delta_{ef}} \sum_{i,j=L,R} \eta_{ij} \frac{g^2}{\Lambda^2_{ij}} (\overline{e}_i \gamma^\mu e_i)(\overline{f}_j \gamma_\mu f_j), \tag{4}$$

where e_i and f_i denote the left- and right-handed initial-state electron and final-state fermion fields. The parameters η_{ij} define the contact interaction model by choosing the contributing helicity amplitudes. By convention $|\eta_{ij}|$ is either zero or one and $g^2/4\pi = 1$, so that all normalisations are absorbed into Λ. The presence of contact interactions leads to modifications of the total and dif-

	$m^{min}_{Z'}$ [GeV]		
Z′ Model	DELPHI	L3	CDF
χ	315	390	595
ψ	330	230	590
η	240	285	620
LR	270	250	630
SSM	–	820	690

Table 4: Lower limits at 95% C.L. on the mass of a Z', independent of the mixing angle $\theta_{\rm M}$. The results from DELPHI and L3 are preliminary.

ferential cross sections:

$$\frac{d\sigma}{d\cos\theta} = \frac{d\sigma^{\mathrm{SM}}}{d\cos\theta} + c_{\mathrm{int}}(s,\cos\theta)\frac{1}{\Lambda^2} + c_{\mathrm{ci}}(s,\cos\theta)\frac{1}{\Lambda^4}. \quad (5)$$

Consequently a fit to the (non-radiative) cross section and asymmetry measurement gives a lower limit on the energy scale at which contact interactions occur. The results of all four LEP experiments [1,2,11,4] are summarised in Figure 6. The 95% C.L. limits obtained vary, depending on the model chosen and the assumption whether the new interaction couples only to leptons or quarks or to all fermions, between about 4 TeV and 10 TeV. However, atomic parity violation experiments place severe constraints on Λ of the order of 15 TeV [12]. The – parity conserving – VV and AA models are not constraint by these measurements.

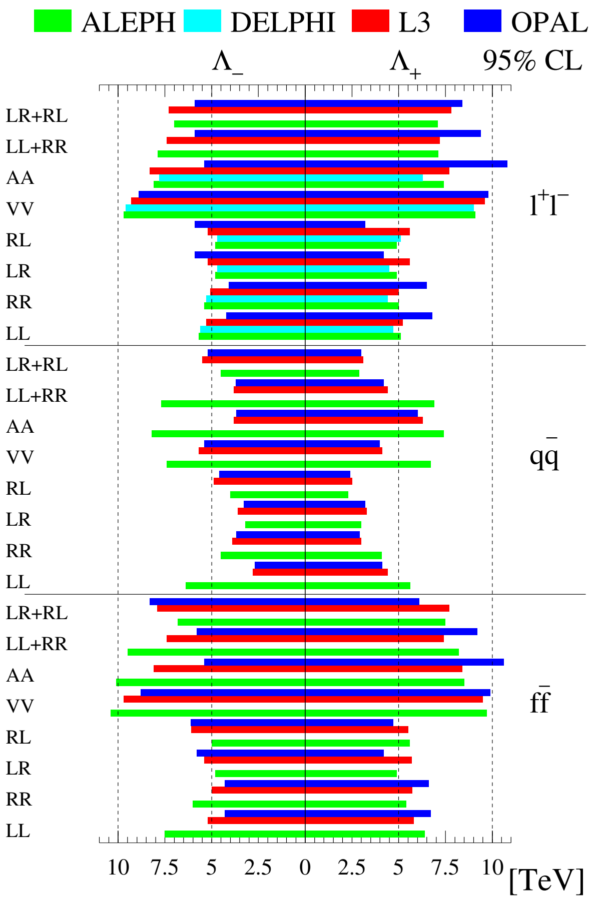

Figure 6: Limits on contact interactions assuming the new interaction couples only to leptons (l^+l^-), to quarks ($q\bar{q}$) or to both.

4 Conclusion

The cross section and asymmetry measurements for fermion pair production at LEP2 energies are in good agreement with the Standard Model predictions. The non-radiative events have been used to confirm the running of the electromagnetic coupling constant α and to improve our knowledge of the interference between γ and Z exchange (j_{had}). Using the data to search for a Z' boson a lower limit on its mass of 240 GeV has been set. In the Sequential Standard model its mass must be higher than 820 GeV. The energy scale for new (contact) interactions has been to constraint to values above 4-10 TeV. Even at the highest energies accessable at e^+e^- colliders today no hint of deviations from the Standard Model has been found.

Acknowledgements

I which to thank the LEP experiments ALEPH, DELPHI, L3 and OPAL for making available their preliminary results at 189 GeV in time.
This work has been supported by the German Bundesministerium für Bildung, Wissenschaft, Forschung und Technologie.

References

1. ALEPH Collab., ICHEP'98 **906**, (1998), ALEPH Collab., ICHEP'98 **908**, (1998).
2. DELPHI Collab., ICHEP'98 **439**, (1998), DELPHI Collab., ICHEP'98 **441**, (1998), DELPHI Collab., ICHEP'98 **643**, (1998).
3. L3 Collab., *Phys. Lett.* B **370**, 195 (1996), L3 Collab., *Phys. Lett.* B **484**, 361 (1997), L3 Collab., ICHEP'98 **484**, (1998), L3 Collab., ICHEP'98 **510**, (1998).
4. OPAL Collab., *Euro. Phys. J.* C **2**, 441 (1998), OPAL Collab., CERN-EP **98-107**, (1998), OPAL Collab., ICHEP'98 **1067**, (1998).
5. OPAL Collab., ICHEP'98 **338**, (1998).
6. A. Leike, T. Riemann and J. Rose, *Phys. Lett.* B **273**, 513 (1991), T. Riemann, *Phys. Lett.* B **293**, 451 (1992).
7. L.S.Durkin, P.Langacker, PLB **166**, 436 (1986), For a review see e.g. J.L.Hewett, T.G.Rizzo, *Phys. Rev.* **183**, 193 (1989), R.N.Mohapatra, "Unifications and Supersymmetries", Springer, New York (1989).
8. L3 Collab., ICHEP'98 **511**, (1998).
9. CDF Collab., *Phys. Rev. Lett.* **79**, 2191 (1997).
10. E.Eichten, K.Lane and M.Peskin, *Phys. Rev. Lett.* **50**, 811 (1983).
11. L3 Collab., ICHEP'98 **513**, (1998).
12. C.S.Wood et al., Science **275**, 1759 (1997), V.Barger, et al., *Phys. Lett.* B **404**, 147 (1997), N.Di Bartolomeo, M.Fabbrichinesi, *Phys. Lett.* B **406**, 237 (1997).